Detection of Pan-Arctic Terrestrial Snowmelt Onset from QuikSCAT, 2000 – 2005

LIBO WANG AND CHRIS DERKSEN[1]

ABSTRACT

Time series of enhanced resolution QuikSCAT scatterometer data were used to detect terrestrial snowmelt onset in the pan-Arctic during the 2000 – 2005 period. Based on the decrease/increase of backscatter upon the appearance/disappearance of liquid water in snow, multiple melt events were identified by a threshold method. Melt events with the longest melt duration or the largest intensity were defined as the primary melt events. There is a good correspondence between the estimated melt onset and air temperature and snow depth observations from WMO weather stations. Maps of the dates of snowmelt onset and the anomalies were produced for each year. The timing of snowmelt onset directly affects the surface energy and water balances, with important implications for the regional to global weather forecasts, carbon source-sink dynamics, and global change assessment and monitoring.

Keywords: snowmelt onset, QuikSCAT, pan-Arctic

INTRODUCTION

Snow cover exists in the northern high latitudes (north of 60º) more than six months each year. A seasonal transition from snow cover to snow free conditions occurs each spring. The timing of snowmelt and the associated thawing of soil in the spring is coincident with the seasonal switch from a net source to sink for atmospheric carbon (Goulden et al., 1998; Jarvis and Linder, 2000). It also affects the stability of permafrost, the length of the active growing season, the surface water and energy balances (e.g., Myneni et al., 1997; Betts et al., 1998; Osterkamp and Romanovsky, 1999; Frolking et al., 2006]. However, mapping of these changes is severely hindered by the sparse network of surface weather stations in the northern high latitudes. Due to its wide swath, satellite-borne microwave scatterometers observe the polar regions multiple times each day in all weather and day/night conditions. The radar backscatter is very sensitive to the appearance/disappearance of liquid water in snow. In this study, data from the SeaWinds scatterometer on QuikSCAT were used to monitor the timing of snowmelt onset across the pan-Arctic landmass for the 2000 – 2005 period.

SATELLITE AND IN SITU DATA

The SeaWinds scatterometer onboard the QuikSCAT satellite was launched in June 1999 and continues to operate at present. It utilizes a conically scanning pencil-beam antenna and makes measurements of the normalized radar cross section (σ^0) at Ku-band (frequency =13.4GHz;

[1]Climate Research Division, Environment Canada, 4905 Dufferin Street, Toronto, Ontario, M3H 5T4 Libo.Wang@ec.gc.ca

wavelength = 2.2cm). It covers 70% of the Earth on a daily basis and provides 90% global backscatter coverage every 2 days with a 0.25 dB relative accuracy [Tsai et al., 2000]. Overlapping orbits at higher latitudes improve the temporal resolution of the instrument, providing multiple σ^0 measurements each day for the polar region, thus allowing reconstruction of surface backscatter at finer spatial resolution. Enhanced resolution products produced from QuikSCAT L1B data with the Scatterometer Image Reconstruction (SIR) algorithm [Long, et al., 1993; Early and Long, 2001; Long and Hicks, 2005] are available twice daily for the pan-Arctic region. The egg-based, horizontal polarization evening pass SIR images were used to detect snowmelt onset in our study. This dataset has a pixel spacing of 4.45 km with an estimated effective resolution of ~ 8-10 km, with approximately 6:00 pm local overpass time.

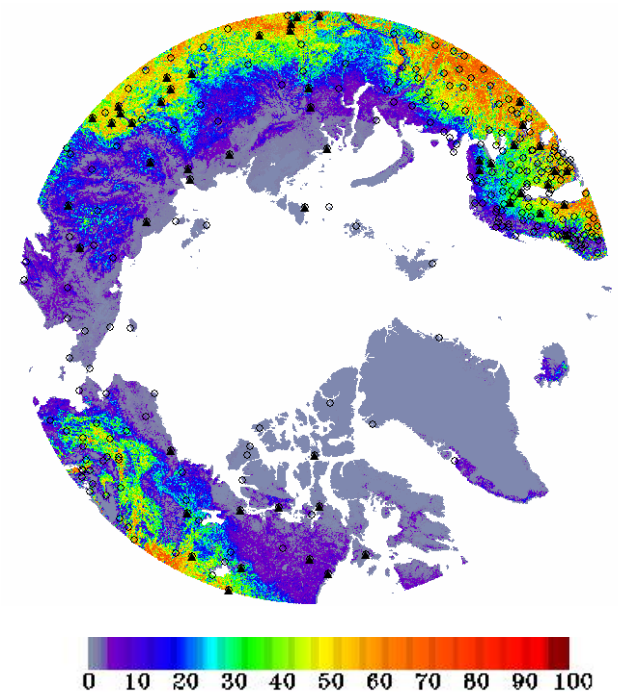

Figure 1. Moderate Resolution Imaging Spectroradiometer (MODIS)-derived tree fraction across the pan-Arctic terrestrial land (Hansen et al., 2003). Black circles represent WMO reporting weather stations with relatively continuous snow depth observations during the 2000 –2005 period. Solid triangles indicate stations with the last snow depth records (in spring) less than 2.0 cm.

The global surface summary of day product produced by the National Climatic Data Center (NCDC, ftp://ftp.ncdc.noaa.gov/pub/data/gsod), consists of 18 surface meteorological elements from World Meteorological Organization (WMO) reporting stations. Air temperature and snow depth observations from circumarctic stations were used to assist in the interpretation of the radar σ^0 data and to develop a snowmelt onset detection algorithm across the pan-Arctic terrestrial land surface (Fig.1). Our study area includes all land areas above 60 ºN degree (Fig.1), covering a broad range of land cover types in different climate regimes, from the cold Arctic tundra (0% tree fraction, grey color in Fig.1) to sparse tundra (purple to blue color in fig.1) to dense boreal forest with a relatively moderate climate (yellow to red color in Fig.1).

METHOD

The basis of melt detection is a dramatic decrease in σ0 at Ku band when there is a small amount of liquid water in snow, while σ0 also increases when the surface refreezes. The basis of our melt detection method is to first look for all the melt events, then identify the primary melt

event. At each pixel, multiple melt events were detected by comparing daily time series of backscatter from days 60 to 200 to a 5-day running mean. The onset of each melt event was identified if the backscatter is 1.7 dB below the mean of the previous five days for three or more consecutive days. The end of the melt event was identified if the backscatter bounced back, making the difference less than 1.7 dB compared to the 5-day mean before the melt onset date. For each melt event, the duration was calculated as the number of days with backscatter 1.7 dB below the 5-day mean. The intensity was defined as the accumulated decrease of σ0 relative to the 5-day mean. Examining the daily snow depth and air temperature observations at representative weather stations (two examples are shown in Fig.2), we found that in most cases melt events with the longest melt duration were responsible for the final ablation of the winter snow pack. Thus we define the melt event with the longest melt duration as the primary melt event. In cases when there were two or more melt events with equal melt duration detected, the melt event with the largest intensity was defined as the primary melt event.

Daily air temperature and snow depth observations at WMO weather stations were used to develop and validate our algorithm. Figure 2(a) shows daily maximum air temperature (blue), snow depth (pink), and backscatter (yellow) data in 2000 for a sparse tundra station (63.20ºN, 14.50ºE). It had a relatively deep snow cover, with maximum snow depth over 60cm. The air temperature fluctuated around 0 ºC degree during the winter, indicating that the station was influenced by a relatively temperate climate. Corresponding to each rise of air temperature to above freezing, there was a dip in backscatter, sometimes associated with a decrease in snow depth. Our algorithm detected 3 melt events from day 60 onward, with melt onset at day 79, 89, and 99 respectively. The corresponding melt duration was 3, 4, and 11 days. The last melt event had the longest melt duration, and was thus considered to be the primary melt event. As noted in Figure 2(a), the primary melt onset date (day 99) is at the early stage of the final melt process. Figure 2(b) shows similar variables for a station with forest cover (65.12ºN, 57.10ºE). A single melt event was detected in this case. The melt onset date was also associated with the early stage of the final ablation of the snow pack.

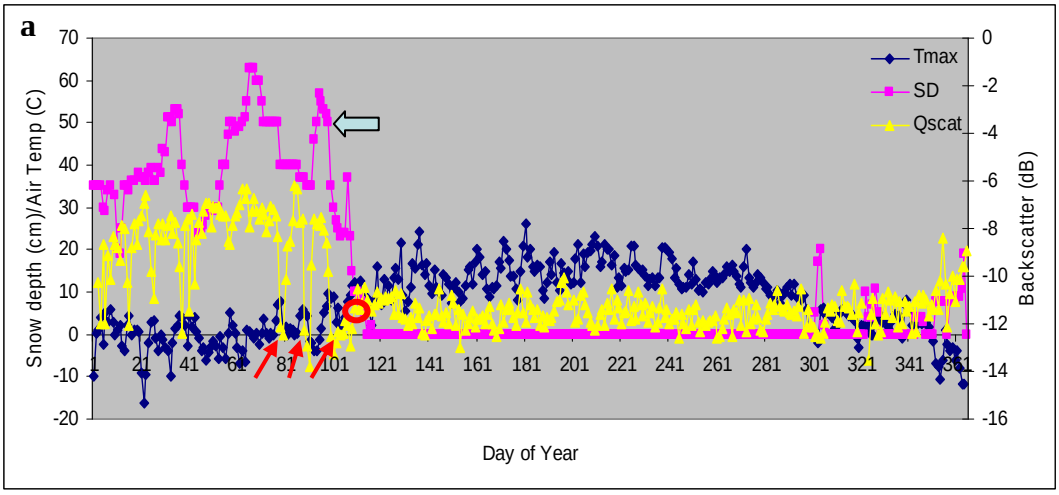

Figure 2. Daily air temperature (blue), snow depth (pink), and backscatter (yellow) at 2 WMO stations : (a) 63.20ºN, 14.50ºE, sparse tundra; (b) 65.12ºN, 57.10ºE, forest cover = 49%. Dates of melt onset are indicated by red arrows, end of snowmelt dates are indicated by red circles, and snow depth values at the estimated primary melt onset dates are indicated by light blue arrows.

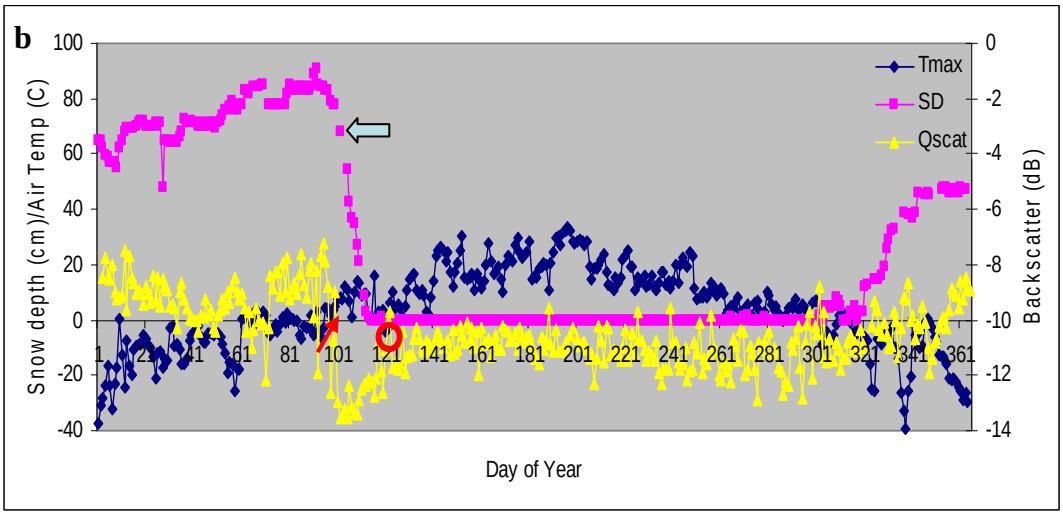

Figure 2 cont. Daily air temperature (blue), snow depth (pink), and backscatter (yellow) at 2 WMO stations : (a) 63.20ºN, 14.50ºE, sparse tundra; (b) 65.12ºN, 57.10ºE, forest cover = 49%. Dates of melt onset are indicated by red arrows, end of snowmelt dates are indicated by red circles, and snow depth values at the estimated primary melt onset dates are indicated by light blue arrows.

RESULTS

Daily mean air temperature at about 200 WMO weather stations across the pan-Arctic region (Fig.1) were used to evaluate the estimated snowmelt onset. For each station, mean air temperature at three dates were extracted from the global summary of the day dataset: (1) on the date of melt onset estimated from QuikSCAT (Fig.3c); (2) one day before the melt onset date (Fig.3b); and (3) two days before the melt onset date (Fig.3a). The number of weather stations available varied in each year - a total number of 1100 air temperature measurements were available for the evaluation during the period 2000 - 2005. The histograms of the air temperature observations (Fig.3) clearly show that a transition from below freezing to above freezing temperature occurred during the 3-day period. This verifies the sensitivity of the developed melt detection algorithm to a temperature transition to above freezing temperatures.

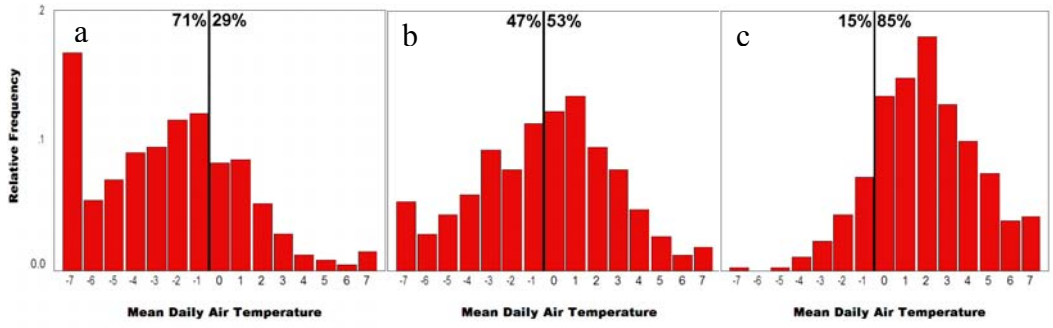

Figure 3. Histogram of daily mean air temperature at weather stations on (a) 2 days before the estimated melt onset date; (b) 1 day before the melt onset date; and (c) the melt onset date.

Dates of snowmelt onset were estimated by applying the above method to the enhanced resolution QuikSCAT data in each spring during the period of 2000 – 2005 (Fig.4). The mean melt onset dates for the 6-year period (Fig. 4g) and the anomaly patterns in each year were calculated (Fig.5). The white coloured areas in Figures 4 and 5 indicate regions with melt not detected from the QuikSCAT data. Analyses of the distribution maps of annual snow depth and vegetation cover

(not shown) indicate that this was most likely due to shallow snow cover or dense forest cover in those areas. The mean melt onset pattern is closely associated with the elevation contours (Fig 4g) – melt onset is later for the high elevation areas (black and pink contours) than the surrounding low elevation areas. On average, melt starts from the middle to the end of March for dense forest regions. As the latitude or elevation increases, the date of melt onset becomes later in the year. For the Arctic tundra, melt does not start until late May to June. The inter-annul variations in the date of melt onset were relatively large for certain regions. For example, in the Canadian Artic tundra mainland, snowmelt onset started roughly in the middle of May in 2001, 2003, and 2005, while it was about one month later in the other years (Fig.4). Across the whole pan-Arctic, the anomalies in snowmelt onset were extremely negative (late) in 2004, in contrast, it was extremely positive (early) in 2005 (Fig.5).

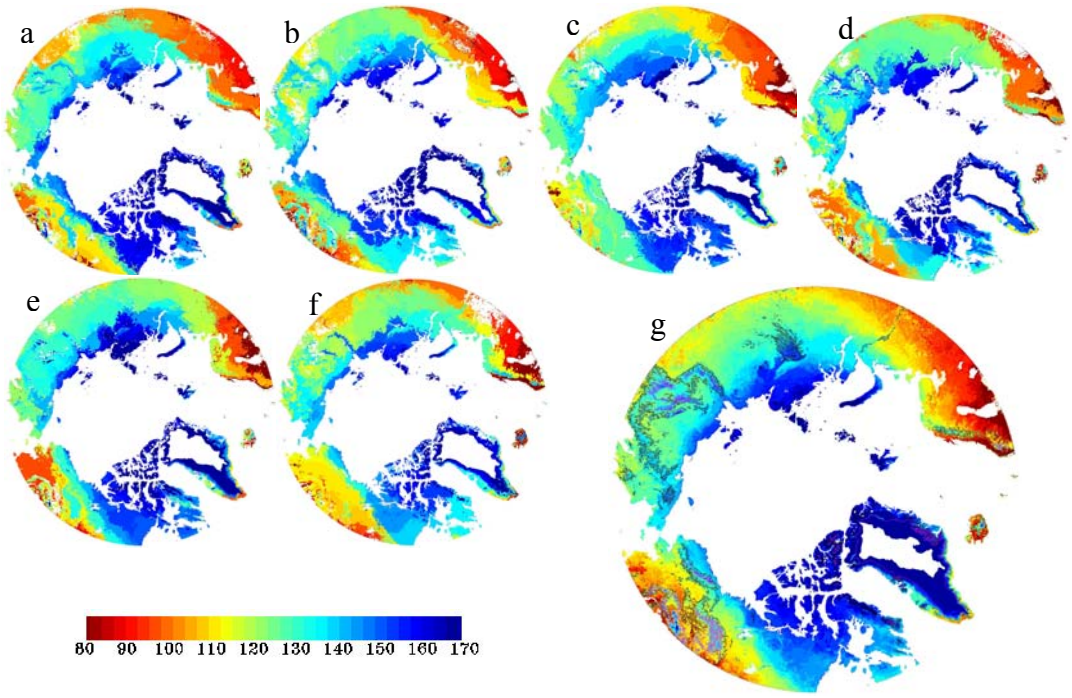

Figure 4. Annual and mean melt onset date for (a) 2000, (b) 2001, (c) 2002, (d) 2003, (e) 2004, (f) 2005, (g) 6-year mean. Black and pink lines represent 700 m a.s.l. and 1500 m a.s.l. elevation contours. White stands for areas with melt not detected from QuikSCAT.

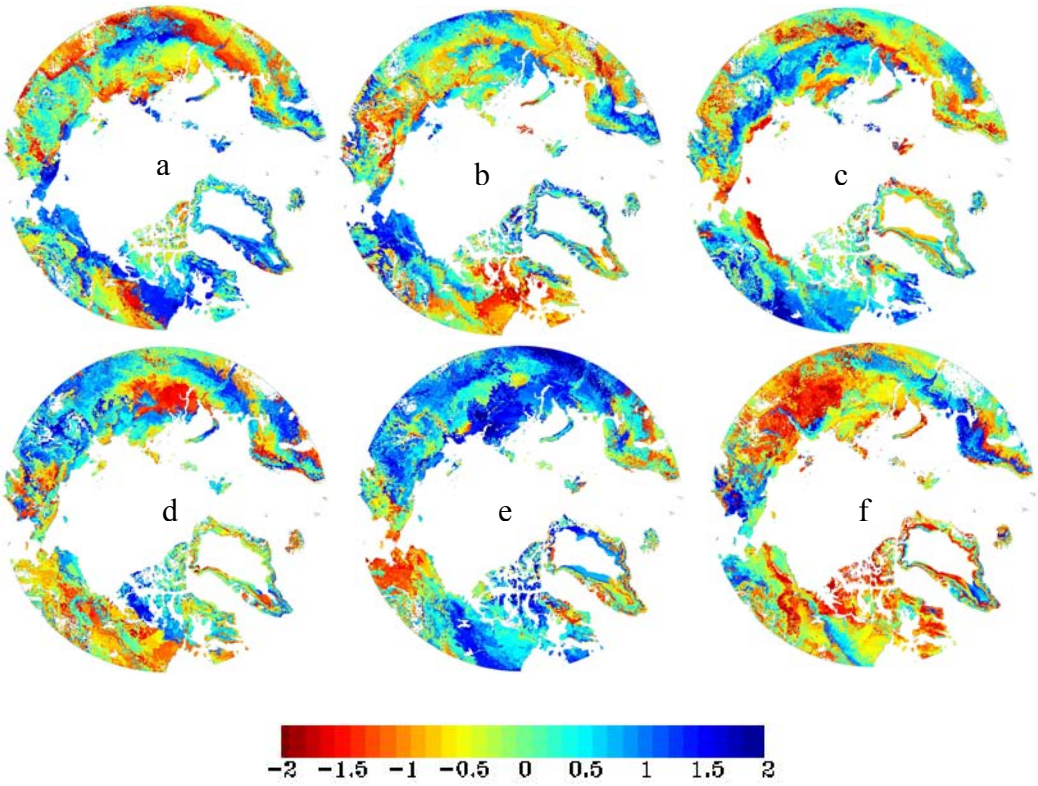

Figure 5. Standard anomalies in melt onset date in (a) 2000, (b) 2001, (c) 2002, (d) 2003, (e) 2004, (f)2005. Red stands for early onset, blue for late onset. White stands for areas with melt not detected from QuikSCAT.

DISCUSSION AND SUMMARY

Due to blowing snow, complex terrain and vegetation conditions, the snow distribution and snowmelt process can be highly heterogeneous in the pan-Arctic (Essery and Pomeroy, 2004; Pomeroy et al., 2006). The melt onset patterns detected from the enhanced resolution QuikSCAT data (4.45 km) in this study are likely to be more accurate than those in previous studies derived from relatively coarse resolution data (25 ~ 50 km) (e.g. Wismann, 2000; Kimball et al., 2001& 2004; Rawlins et al., 2005). In addition, the method used in this study was evaluated using observations from weather stations distributed across the whole pan-Arctic region, while previous methods were either applied to a limited area or only validated from limited in situ observations.

Multiple melt events and the primary melt onset were detected from the enhanced resolution QuikSCAT scatterometer data for the period 2000 – 2005. The results reveal large annual and inter-annual variations in the terrestrial snowmelt onset across the pan-Arctic region. Analysis of daily air temperature from 200 WMO reporting weather stations across the pan-Arctic region indicate that the algorithm did capture the transition period from freezing to above freezing conditions. The timing of snowmelt onset directly affects the surface-atmosphere energy, carbon, and water exchange. Improved algorithms applied to enhanced resolution data for monitoring the spring seasonal transition in the northern high latitude land may therefore be potentially important for regional to global weather forecasts, carbon source-sink dynamics, river discharge/runoff and global change studies.

ACKNOWLEDGMENTS

We would like to thank the following data providers: NASA Scatterometer Climate Record Pathfinder Project for enhanced resolution QuikSCAT data; NOAA NCDC for Global summary of the day data; Global Land Cover Facility for MODIS Vegetation; and Ross Brown and Bruce Brasnett for CMC Daily Snow Depth Analysis.

REFERENCES

Betts, A. K., Viterbo, P., Beljaars, A., Pan, H.-L., Hong, S.-Y., Goulden, M., and Wofsy, S. 1998. Evaluation of land-surface interaction in ECMWF and NCEP/NCAR reanalysis models over grassland (FIFE) and boreal forest (BOREAS). *Journal of Geophysical Research* **103**(D18): 23079– 23085.

Early D. S., and D. G. Long. 2001. Image Reconstruction and Enhanced Resolution Imaging from Irregular Samples. *IEEE Transactions on Geoscience and Remote Sensing* **39** (2): 291-302.

Essery R. L. H., and J. W. Pomeroy. 2004. Vegetation and topographic control of wind-blown snow distributions in distributed and aggregated simulations for an arctic tundra basin. *Journal of Hydrometeorology* **5**: 734–744.

Frolking, S., T. Milliman, K. McDonald, J. Kimball, M. Zhao, and M. Fahnestock. 2006. Evaluation of the SeaWinds scatterometer for regional monitoring of vegetation phenology, *J. Geophys. Res*. **111:** D17302, doi:10.1029/2005JD006588.

Goulden, M. L., Wofsy, S. C., Harden, J. W., Trumbore, S. E., Crill, P. M., Gower, S. T., Fries, T., Daube, B. C., Fan, S.-M., Sutton, D. J., Bazzaz, A., and Munger, J. W. 1998. Sensitivity of boreal forest carbon balance to soil thaw. *Science* **279:** 214– 217.

Hansen, M., R. DeFries, J. Townshend, M. Carroll, C. Dimiceli, R. Sohlberg. 2003. Global percent tree cover at a spatial resolution of 500 meters: first results of the MODIS vegetation continuous fields algorithm. *Earth Interactions* **7(10):** 1–15.

Jarvis, P., and Linder, S. 2000. Constraints to growth of boreal forests. *Nature* **405**: 904– 905.

Kimball, J. S., McDonald, K. C., Keyser, A. R., Frolking, S., & Running, S. W. 2001. Application of the NASA Scatterometer (NSCAT) for determining the daily frozen and non-frozen landscape of Alaska. *Remote Sensing of Environment* **75:** 113– 126.

Kimball, J.S., McDonald, K.C., Frolking, S., Running, S.W. 2004. Radar remote sensing of the spring thaw transition across a boreal landscape. *Remote Sensing of Environment* **89:** 163–175.

Long, D. G., P. J. Hardin, and P. T. Whiting. 1993. Resolution enhancement of spaceborne scatterometer data, *IEEE Transactions on Geoscience and Remote Sensing* **32:** 700-715.

Long, D. G., and B. R. Hicks. 2005. Standard BYU QuikSCAT/SeaWinds land/ice image products, report, Brigham Young Univ., Provo, Utah.

Myneni, R. B., C. D. Keeling, C. J. Tucker, G. Asrar, and R. R. Nemani. 1997. Increased plant growth in the northern high latitudes from 1981 to 1991, *Nature* **386**: 698– 702.

Pomeroy, J. W., D. S. Bewley, R. L. H. Essery, N. R. Hedstrom, T. Link, R. J. Granger, J. E. Sicart, C. R. Ellis1 and J. R. Janowicz. 2006. Shrub tundra snowmelt. *Hydrol. Process.* **20**: 923–941.

Rawlins, M., K. McDonald, S. Frolking, R. Lammers, M. Fahnestock, J. Kimball, and C. Vorosmarty. 2005. Remote sensing of pan-Arctic snowpack thaw using the SeaWinds scatterometer, *J. Hydrol.,* **312:** 211 –294.

Tsai, W.-Y., S. V. Nghiem, J. N. Huddleston, M. W. Spencer, B. W. Stiles, and R. D.West. 2000. Polarimetric scatterometry: A promising technique for improving ocean surface wind measurements*, IEEE Transactions on Geoscience and Remote Sensing* **38(4):** 1903– 1921.

Wismann, V. (2000), Monitoring of seasonal thawing in Siberia with ERS scatterometer data, IEEE Trans. Geosci. *Remote Sens,* **38**: 1804– 1809.